Intermittency route to strange nonchaotic attractors in a non-skew-product map

Takahito Mitsui* and Yoji Aizawa
Department of Applied Physics, Waseda University, Tokyo 169-8555, Japan
(Received 26 October 2009; revised manuscript received 21 March 2010; published 21 April 2010)

Whether strange nonchaotic attractors (SNAs) can typically arise in non-skew-product maps has been a crucial question for more than two decades. Recently, it was shown that SNAs arise in a particular non-skew-product map related to quasiperiodically driven continuous dynamical systems [R. Badard, Chaos, Solitons Fractals **28**, 1327 (2006); Chaos **18**, 023127 (2008)]. In the present paper, we derive Badard's non-skew-product map from a periodically driven continuous dynamical system with spatially quasiperiodic potential and investigate onset mechanisms of SNAs in the map. In particular, we focus on a transition route to intermittent SNAs, where SNAs appear after pair annihilations of stable and unstable fixed points located on a ring-shaped invariant curve. Then the mean residence time and rotation numbers have a logarithmic singularity. Finally, we discuss the existence of SNAs in a special class of non-skew-product maps.

DOI: 10.1103/PhysRevE.81.046210 PACS number(s): 05.45.Ac, 05.45.Pq

I. INTRODUCTION

Strange nonchaotic attractors (SNAs) are nontrivial attractors lying between quasiperiodicity and chaos. The concept of SNAs was introduced by Grebogi *et al.* [1], and since then SNAs have been investigated theoretically [1–25] as well as experimentally [25–28] (for recent reviews, see [29,30]). According to the definition by Grebogi *et al.* [1], here the term "strange attractor" means a piecewise nondifferentiable attractor which is neither a finite set of points, a closed curve, a piecewise smooth surface, nor a volume bounded by a piecewise smooth closed surface. The term "nonchaotic" means that the maximum Lyapunov exponent is nonpositive; that is, there is no exponential sensitivity to initial conditions.

SNAs appear to be *typical* in quasiperiodically driven dynamical systems [1,2] as well as in quantum systems with a spatially quasiperiodic potential [3,4]. That is, SNAs exist over sets of positive measure in parameter space in these systems [31]. In general, a quasiperiodically driven continuous dynamical system is transformed into a map of *skew-product* type [32],

$$x_{n+1} = g(x_n, \theta_n),$$

$$\theta_{n+1} = \theta_n + \omega \pmod 1, \tag{1}$$

where the function $g(x,\theta)$ is periodic in θ, and ω is irrational. However, the same continuous system can be transformed into a map without skew-product structure.

As discussed in previous papers [6] the following questions are not yet clear: (Q1) Are there any periodically forced or autonomous systems which typically exhibit SNAs? (Q2) Are there any non-skew-product maps which typically exhibit SNAs? (Q3) If SNAs arise in any non-skew-product maps, what kinds of new phenomena can be observed? Grebogi *et al.* noted that SNAs are not robust against small perturbations which destroy the skew-product structure [1]. Wang *et al.* showed that SNAs are induced in non-skew-product maps by the addition of noise [8], but these systems can be considered as skew-product if the dynamics of the noise is included as a part of system definition.

Recently, Badard showed that some quasiperiodically driven continuous systems can be transformed both into skew-product maps and into non-skew-product maps by considering different Poincaré sections and gave a positive answer to question (Q2) by presenting a non-skew-product map which generates SNAs [9,10]. In the present paper, we will explore Badard's non-skew-product map obtained from a different physical origin and show a type of intermittency route to SNAs. Several types of intermittency routes to SNAs are known to exist, where smooth tori collapse and transform into intermittent SNAs [16–25]. On the other hand, in Badard's map, the transition to intermittent SNAs can occur after pair annihilations of stable and unstable fixed points located on a ring-shaped invariant curve. Our results not only support Badard's answer to question (Q2) but also give an answer to question (Q3) although question (Q1) is still open.

This paper is organized as follows. In Sec. II, we give a short review of Badard's map and explicitly derive the same map from a physical toy model. Then we can remove two assumptions on invertibility and on absence of fixed point from Badard's construction [9]. The removal of the latter assumption is a key to the type of intermittency transition to SNAs. In Sec. III, a characterization method for SNAs is explained. In Sec. IV, we present numerical results to show the existence of SNAs in the map and demonstrate the intermittency transition to SNAs. A summary and discussion are provided in Sec. V.

II. MODEL

A. Brief review of Badard's map

In the beginning, we briefly review Badard's map in [9,10]. Consider the quasiperiodically driven oscillator defined by the following differential equation on $\mathbb{R}^3$:

$$\dot{x} = 1 + aF(x,y,z),$$

$$\dot{y} = \alpha,$$

*takahito321@ruri.waseda.jp

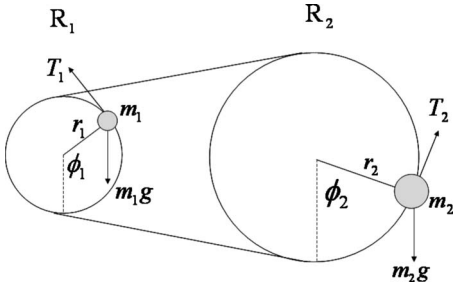

FIG. 1. Incommensurately coupled kicked rotators. See text for notation.

$$\dot{z} = \beta, \tag{2}$$

where F is Lipchitz and periodic in x, y, and z with period 1, and β/α is irrational. Suppose $|F| \leq 1$ and $|a| < 1$ so that x is always increasing. This system can be defined on the 3-torus by taking modulo 1 for x, y, and z.

To analyze such a flow system we commonly construct stroboscopic maps by the Poincaré section method. It is usual to discretize Eq. (2) in either period of drivings. Then we obtain a map of skew-product type in Eq. (1). Another discretization way is to consider the instants t_n at which the variable x takes integer values, $x(t_n) \in \mathbb{Z}$. The time $(t_{n+1}-t_n)$ necessary for x to increase by 1 is defined by a single function $\tau(y_n, z_n)$, where $y(t_n)=y_n$ and $z(t_n)=z_n$. From linear evolutions of y and z, we obtain a map of *non-skew-product* type on $\mathbb{R}^2$,

$$y_{n+1} = y_n + \alpha\tau(y_n, z_n),$$

$$z_{n+1} = z_n + \beta\tau(y_n, z_n). \tag{3}$$

Equation (3) can be defined on 2-torus $\mathbb{T}^2$ by taking modulo 1 for y and z. As proven in [9], function $\tau(y,z)$ is continuous, periodic in y and z, strictly positive and bounded, and map (3) is a *homeomorphism* both on $\mathbb{R}^2$ and $\mathbb{T}^2$ (i.e., an invertible map). Furthermore, map (3) can neither have fixed points nor cycles, and it has only a rotation vector independent of initial conditions. Badard chose

$$\tau(y,z) = K + \frac{H}{2\pi\alpha}\sin(2\pi y) + \frac{Q}{2\pi\beta}\sin(2\pi z) \tag{4}$$

for numerical experiments and showed that the non-skew-product map exhibits SNAs [9,10].

B. Derivation of Badard's map

To derive Badard's map in Eqs. (3) and (4) explicitly, we consider the motion of two incommensurately coupled rotators, R_1 and R_2, driven by periodic kicks (see Fig. 1). Each rotator has rotational angle $\phi_i \in \mathbb{R}$ and radius r_i $(i=1,2)$. The rotaters are coupled by a stiff rope and rotate satisfying a restraint $\phi_2 = k\phi_1 + \delta$, where $k=r_1/r_2$ is *irrational*, and $\delta \in \mathbb{R}$ is the value of ϕ_2 at $\phi_1=0$. Each rotator accompanies a point mass m_i at a fixed position on the circumference, and each mass is kicked by a gravitational force $m_i g$ and a rotative force T_i with a period of t_p. In addition, each mass is subjected to a damping force with coefficient γ_i. Then the dimensionless equations of angles are

$$\ddot{\phi}_1 = -\eta\dot{\phi}_1 + [T - \sin\phi_1 - a\sin(k\phi_1 + \delta)]\sum_n \delta(t - \tau n),$$

$$\phi_2 = k\phi_1 + \delta, \tag{5}$$

or equivalently

$$\ddot{\phi}_1 = -\eta\dot{\phi}_1 + (T - \sin\phi_1 - a\sin\phi_2)\sum_n \delta(t - \tau n),$$

$$\ddot{\phi}_2 = -\eta\dot{\phi}_2 + k(T - \sin\phi_1 - a\sin\phi_2)\sum_n \delta(t - \tau n), \tag{6}$$

with $\dot{\phi}_2(0) = k\dot{\phi}_1(0)$ and $\phi_2(0) = k\phi_1(0) + \delta$, where time is scaled by the characteristic time $t_c = \{(1+m_2/m_1)r_1/g\}^{1/2}$, and the other parameters are given by $\eta = (\gamma_1+\gamma_2)r_1 t_c^{-1/2}/m_1 g$, $T = (T_1+T_2)/m_1 g$, $a = m_2/m_1$, and $\tau = t_p/t_c$.

Integrating Eq. (5) over a period τ from $t = n\tau - \varepsilon$ to $t = (n+1)\tau - \varepsilon$, we obtain a map for the variables $(v_n, \phi_n) := \lim_{\varepsilon\to 0}(\dot{\phi}_1(n\tau-\varepsilon), \phi_1(n\tau-\varepsilon))$,

$$v_{n+1} = e^{-\eta\tau}[v_n + T - \sin\phi_n - a\sin(k\phi_n + \delta)],$$

$$\phi_{n+1} = \phi_n + \frac{1 - e^{-\eta\tau}}{\eta}[v_n + T - \sin\phi_n - a\sin(k\phi_n + \delta)]. \tag{7}$$

This map has a Jacobian $-e^{-\eta\tau}$ and is invertible for finite τ. In the overdamped limit $\tau(=t_p/t_c) \to \infty$, map (7) becomes noninvertible due to a loss of memory about previous state, and it is reduced to a one-dimensional map $f: \mathbb{R} \to \mathbb{R}$ for the variable $x_n = -\phi_n/2\pi$,

$$x_{n+1} = x_n + \Omega + \frac{V}{2\pi}\left(\sin 2\pi x_n + \frac{\alpha}{k}\sin 2\pi(kx_n + \theta)\right),$$

$$:= f(x_n; \theta), \tag{8}$$

where $V = 1/\eta$, $\Omega = -T/2\pi\eta$, $\theta = -\delta/2\pi$, and $\alpha = ka$. This map is invertible for $V \leq V_c[:= 1/(1+\alpha)]$ and noninvertible for $V > V_c$. Note that map f reduces to the well-known sine-circle map for $\alpha = 0$. When we regard θ as a system's "variable," we deal with an extended map $F: \mathbb{R}^2 \to \mathbb{R}^2$ such that

$$(x_{n+1}, \theta) = F(x_n, \theta) := (f(x_n; \theta), \theta).$$

In the same manner of integration, Eq. (6) yields a two-dimensional map $M: \mathbb{R}^2 \to \mathbb{R}^2$ for the variable $(y_n, z_n) := \lim_{\varepsilon\to 0}(-\phi_1(n\tau-\varepsilon)/2\pi, -\phi_2(n\tau-\varepsilon)/2\pi)$ in the overdamped limit

$$M: \begin{cases} y_{n+1} = y_n + \Omega + \dfrac{V}{2\pi}\left(\sin 2\pi y_n + \dfrac{\alpha}{k}\sin 2\pi z_n\right) \\ z_{n+1} = z_n + k\left[\Omega + \dfrac{V}{2\pi}\left(\sin 2\pi y_n + \dfrac{\alpha}{k}\sin 2\pi z_n\right)\right] \end{cases}.$$

Again we have a restraint for these variables,

$$z_n = ky_n + \theta. \tag{9}$$

The maps F and M are *topologically conjugate* by the homeomorphism h given by

$$(y_n, z_n) = h(x_n, \theta) := (x_n, kx_n + \theta). \tag{10}$$

Hence, the dynamics of map M can be explored by the rather simple map F. Map M can be defined on $\mathbb{T}^2$. Denote by $\tilde{M}$ the map of $\mathbb{T}^2$ obtained by taking modulo 1 for y and z in M,

$$\tilde{M}: \begin{cases} y_{n+1} = y_n + \Omega + \dfrac{V}{2\pi}\left(\sin 2\pi y_n + \dfrac{\alpha}{k}\sin 2\pi z_n\right) \\ \quad (\mathrm{mod}\ 1), \\ z_{n+1} = z_n + k\left[\Omega + \dfrac{V}{2\pi}\left(\sin 2\pi y_n + \dfrac{\alpha}{k}\sin 2\pi z_n\right)\right] \\ \quad (\mathrm{mod}\ 1). \end{cases}$$

Then map M is called a *lift* of map $\tilde{M}$. Map $\tilde{M}$ corresponds with Badard's map, Eqs. (3) and (4), with parameter changes. However, we can reasonably consider noninvertible and fixed points regimes in map $\tilde{M}$, unlike in Badard's map.

In this paper, we are interested in attractors of map $\tilde{M}$, especially in SNAs. We will recall other related maps f, F or M when needed. In what follows, consider Ω and V as control parameters. We can set $\Omega \geq 0$ without loss of generality, and $V > 0$ by definition.

As with map f, map $\tilde{M}$ is also invertible for $V \leq V_c$ and noninvertible for $V > V_c$. In the invertible region $V \leq V_c$, the rotation numbers of y and z with respect to lift M are defined without dependence on initial conditions [9]:

$$W_y = \lim_{n\to\infty}(y_n - y_0)/n, \quad W_z = \lim_{n\to\infty}(z_n - z_0)/n. \tag{11}$$

From Eq. (9), the rotation numbers satisfy $W_z = kW_y$. In the noninvertible region $V > V_c$, the rotation numbers may depend on the initial conditions [10].

For $\Omega < \Omega_b(V)[:= \frac{V}{2\pi}(1+\frac{\alpha}{k})]$, fixed points are the only possible attractors if $V < V_c$, and in contrast, some cycles or chaotic attractors can coexist with fixed points if $V > V_c$. This fixed points region $\Omega < \Omega_b(V)$ cannot appear in Badard's construction. On the other hand, for $\Omega > \Omega_b(V)$, map $\tilde{M}$ has neither fixed points nor any cycles as shown in [33]. Thus, map $\tilde{M}$ should exhibit some quasiperiodic or aperiodic motion for $\Omega > \Omega_b(V)$.

III. CHARACTERIZATION METHOD

Firstly, we look at the Lyapunov spectrum of map $\tilde{M}$ and show that one exponent is always zero, and that the other exponent corresponds with the Lyapunov exponent of map f. For map $\tilde{M}$, the Lyapunov exponent for an initial tangent vector u_0 is given by

$$\lim_{n\to\infty}\frac{1}{n}\ln\|D\tilde{M}^n(y_0, z_0)u_0\|, \tag{12}$$

where $D\tilde{M}^n(y_0, z_0)$ is the Jacobian matrix of the nth iterated map $(y_n, z_n) = \tilde{M}^n(y_0, z_0)$ given by

$$D\tilde{M}^n(y_0, z_0) = \begin{pmatrix} \dfrac{\partial y_n}{\partial y_0} & \dfrac{\partial y_n}{\partial z_0} \\ \dfrac{\partial z_n}{\partial y_0} & \dfrac{\partial z_n}{\partial z_0} \end{pmatrix}.$$

Using Eq. (10), we can transform this matrix into

$$D\tilde{M}^n(y_0, z_0) = \begin{pmatrix} \dfrac{\partial x_n}{\partial x_0} - k\dfrac{\partial x_n}{\partial \theta} & \dfrac{\partial x_n}{\partial \theta} \\ k\left(\dfrac{\partial x_n}{\partial x_0} - k\dfrac{\partial x_n}{\partial \theta}\right) - k & k\dfrac{\partial x_n}{\partial \theta} + 1 \end{pmatrix}.$$

One can easily see that the Jacobian matrix $D\tilde{M}^n(y_0, z_0)$ has an eigenvector $(1, k)$ with eigenvalue $\frac{\partial x_n}{\partial x_0}$. Thus, the Lyapunov exponent for $u_0 = (1, k)$ is

$$\lim_{n\to\infty}\frac{1}{n}\ln\left|\frac{\partial x_n}{\partial x_0}\right| = \lim_{n\to\infty}\frac{1}{n}\sum_{j=0}^{n-1}\ln|f_x(x_j;\theta)| \equiv \lambda_f, \tag{13}$$

where λ_f is the Lyapunov exponent of map f. Equation (12) can take at most two different values depending on the initial tangent vector u_0. We denote the other Lyapunov exponent by $\bar{\lambda}$. Then these exponents λ_f and $\bar{\lambda}$ satisfy

$$\lambda_f + \bar{\lambda} = \lim_{n\to\infty}\frac{1}{n}\ln|\det D\tilde{M}^n(y_0, z_0)|.$$

Using $\det D\tilde{M}^n(y_0, z_0) = \partial x_n/\partial x_0$, we obtain $\lambda_f + \bar{\lambda} = \lambda_f$; that is, Lyapunov exponent $\bar{\lambda}$ is always zero. Therefore, the attractor of map $\tilde{M}$ is chaotic (or nonchaotic) if the Lyapunov exponent λ_f is positive (or nonpositive). Note that other maps M and F have the same Lyapunov spectrum $\{\lambda_f, 0\}$.

Secondly, to discuss the strangeness of nonchaotic attractors with $\lambda_f < 0$, let us look at the evolution of infinitesimal perturbation $\delta\mathbf{u}_n = (\delta y_n, \delta z_n)$ of an orbit (y_n, z_n), which is governed by $\delta\mathbf{u}_n = D\tilde{M}^n(y_0, z_0)\delta\mathbf{u}_0$. Orthogonal transformation by the matrix $U = 1/\sqrt{k^2+1}\begin{pmatrix} k & -1 \\ 1 & k \end{pmatrix}$ yields $\delta\mathbf{u}'_n = UD\tilde{M}^n(y_0, z_0)U^{-1}\delta\mathbf{u}'_0$, where $\delta\mathbf{u}'_n = U\delta\mathbf{u}_n$ and $UD\tilde{M}^n(y_0, z_0)U^{-1} = \begin{pmatrix} 1 & 0 \\ k\partial x_n/\partial x_0 - (k^2+1)\partial x_n/\partial\theta - k & \partial x_n/\partial x_0 \end{pmatrix}$. For the case $\lambda_f < 0$, the derivative $|\partial x_n/\partial x_0| \sim e^{\lambda_f n}$ is exponentially small for large n, and the perturbation for large n is approximated by

$$\delta\mathbf{u}'_n \approx \delta y'_0 \begin{pmatrix} 1 \\ -(k^2+1)\dfrac{\partial x_n}{\partial\theta} - k \end{pmatrix}.$$

The phase derivative $\partial x_n/\partial\theta$ in the perturbation equation is given by the recurrence relation

$$\frac{\partial x_{n+1}}{\partial\theta} = f_x(x_n;\theta)\frac{\partial x_n}{\partial\theta} + f_\theta(x_n;\theta) \tag{14}$$

from Eq. (8). For large n, unperturbed and perturbed orbits, (y'_n, z'_n) and $(y'_n + \delta y'_n, z'_n + \delta z'_n)$, converge to orbits on an attractor, respectively, and the ratios $\delta z'_n/\delta y'_n \approx -(k^2+1)\partial x_n/\partial\theta - k$ given by the perturbation equation tend to the derivatives of the attractor along a trajectory in the rotated

coordinate (y',z'). That is, the strangeness of attractors can be measured by the asymptotic behavior of $|\delta z_n'/\delta y_n'|$. This leads to the same criterion introduced by Pikovsky and Feudel [12]: if the phase derivative $|\partial x_n/\partial\theta|$ is bounded for all n, the attractor is smooth; on the other hand, if the phase derivative $|\partial x_n/\partial\theta|$ can be arbitrarily large along a trajectory (i.e., unbounded), the attractor cannot be smooth. Following Pikovsky and Feudel [12], we can evaluate the strangeness of an attractor by the phase sensitivity function $\Gamma(n)$,

$$\Gamma(n) = \min_{x_0,\theta}\left[\max_{1\le k\le n}\left|\frac{\partial x_k}{\partial\theta}\right|\right].$$

This quantity is known to behave as $\Gamma(n)\sim n^{\nu}(\nu>0)$ asymptotically for SNAs, where ν is called the phase sensitivity exponent [12,29]. Therefore, we can say that map $\tilde{M}$ has an SNA for the case $\lambda_f<0$ and $\nu>0$. In this paper, we do not consider the possibility of $\lambda_f=0$ and $\nu>0$ (i.e., *critical* SNAs [5]) since the set of parameter values yielding such exponents has Lebesgue measure zero in general.

IV. NUMERICAL RESULTS

In what follows, we set $k=(\sqrt{5}-1)/2$ and $\alpha=0.5$, and numerically study attractors of map $\tilde{M}$ focusing on bifurcation phenomena in the invertible region $V\le V_c(=2/3)$. The phenomena occurred in the noninvertible region will be reported elsewhere [34].

A. Phase diagram in Ω-V plane

Figure 2 shows the phase diagram for map $\tilde{M}$. Each phase is characterized by the Lyapunov exponent λ_f and phase sensitivity exponent ν. In the region $\Omega<\Omega_b(V)$ denoted by *FP* and shown in black, only possible attractors are fixed points. In contrast, several types of attractors with nonzero rotation numbers appear for $\Omega>\Omega_b(V)$. Quasiperiodic attractors on one or more smooth curves exist in the tonguelike regions denoted by $T1$ and also shown in black. Hereafter, we call such an attractor a "1-torus" (of single or multiband). 1-torus has $\lambda_f<0$ and $\nu=0$. Quasiperiodic attractors on the whole 2-torus exist in invertible regions between the $T1$-tongues, which are denoted by $T2$ and shown in blue. Hereafter, we call such an attractor a "2-torus." 2-torus has $\lambda_f=0$ and $\nu=0$. Chaotic attractors with $\lambda_f>0$ exist in the noninvertible region denoted by *Ch* and shown in red. SNAs with $\lambda_f<0$ and $\nu>0$ exist in border regions of $T1$-tongues which are denoted by *SNA* and shown in green. The numerical criteria for 1-torus, 2-torus, SNA, and chaotic attractor are $\lambda_f<-10^{-5}$ and $\nu<0.1$, $|\lambda_f|<10^{-5}$, $\lambda_f<-10^{-5}$ and $\nu>0.1$, $\lambda_f>10^{-5}$, respectively. The Lyapunov exponent λ_f is calculated for 2×10^6 iterations after discarding the initial 5×10^3 transients, and the phase sensitivity exponent ν is determined from the growth rate of $\log\Gamma(n)$ between the time interval $[10^5,10^7]$.

In regions *FP* and $T1$, the dynamics are mode locked; that is, the rotation numbers satisfy

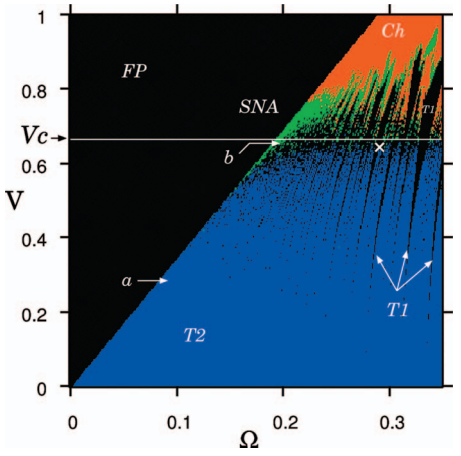

FIG. 2. (Color) Phase diagram in the Ω-V plane for map $\tilde{M}$. Regions of fixed points (*FP*) and 1-torus ($T1$), 2-torus ($T2$), strange nonchaotic attractor (*SNA*), and chaotic attractor (*Ch*) are shown in black, blue, green, and red, respectively. Solid line represents $V_c=2/3$ and divides the plane into invertible (below) and noninvertible (above) regions. Cross (×) shows the nonsmooth saddle-node bifurcation point near $\Omega^*=0.294\,067\,34$, $V=0.666$ discussed in the text. When crossing the boundary of *FP* [given by $\Omega=\Omega_b(V) := \frac{V}{2\pi}(1+\frac{\alpha}{k})$], fixed points transit to an intermittent attractor: 2-torus (route a), SNA (route b), or chaotic attractor.

$$W_y=\frac{m}{n}+\frac{l}{n}\frac{1}{k} \quad \text{and} \quad W_z=\frac{m}{n}k+\frac{l}{n}, \tag{15}$$

where m, l, and n are integers. Multiplicities of a single curve in 1-torus in the y-and z-directions have a ratio $|m/l|$, but the triplet (m,l,n) itself is not determined by the apparent configuration of a 1-torus. Note that the regions *FP* and $T1$ are contained in the mode-locking regions, so-called Arnol'd tongues, but not all the mode-locking regions are *FP* or $T1$, as some SNAs and chaotic attractors can also satisfy the mode-locking condition (cf. [13,19]).

B. Nonsmooth saddle-node bifurcation route to SNAs

As reported in [9], map $\tilde{M}$ exhibits transitions from a 1-torus to an SNA due to the *nonsmooth saddle-node bifurcation of tori* [13]. When the parameters cross the boundary of $T1$-tongues, a 1-torus can transit to an SNA through a collision with an unstable 1-torus. One of such transition points is located near $\Omega^*=0.294\,067\,34$, $V=0.666$, which is denoted by the cross (×) in Fig. 2. Figure 3(a) shows a 7-band 1-torus (fat dots) with $\lambda_f=-0.004\,863$ and $\nu=0$, and an unstable 7-band 1-torus (dots) for $\Omega=0.294\,060$, $V=0.666$. Figure 3(b) shows an SNA with $\lambda_f=-0.000\,406$ and $\nu=1.03$ for $\Omega=0.294\,067\,4$, $V=0.666$. The mode-locking condition breaks through the nonsmooth saddle-node bifurcation. Indeed, the rotation number of y changes its value from $W_y=(-3+3/k)/7\approx0.264\,871\,7$ to $W_y\approx0.264\,879\,0$.

C. Intermittency route to SNAs

Besides the nonsmooth saddle-node bifurcation, another type of transition to SNAs occurs in the invertible region

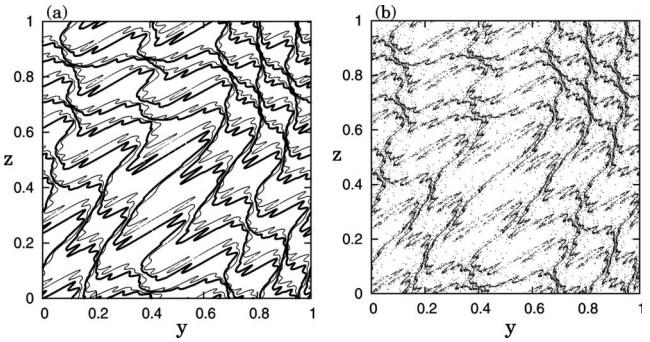

FIG. 3. Emergence of an SNA due to the nonsmooth saddle-node bifurcation near $\Omega^*=0.294\,067\,34$, $V=0.666$: (a) Stable 7-band 1-torus (fat dots) and unstable 7-band 1-torus (dots) for $\Omega=0.294\,060$, $V=0.666$; (b) SNA for $\Omega=0.294\,067\,4$, $V=0.666$.

when the parameters cross the boundary $\Omega=\Omega_b(V)$ (see route *b* in Fig. 2). In region *FP*, fixed points exist on one or more invariant curves given by $\sin(2\pi y)+\frac{\alpha}{k}\sin(2\pi z)=-\frac{2\pi\Omega}{V}$ in phase space [see Fig. 4(a)]. By the linear stability analysis for the fixed points, one can proves that the phase space is divided into contracting and expanding regions by critical curves given by $\Lambda(y,z):=\cos(2\pi y)+\alpha\cos(2\pi z)=0$. That is, fixed points are stable for $\Lambda(y,z)<0$ and unstable for $\Lambda(y,z)>0$. For the case $\Omega<\frac{V}{2\pi}(1-\frac{\alpha}{k})$, the stable (solid line) and unstable (dotted line) fixed points are separated by two

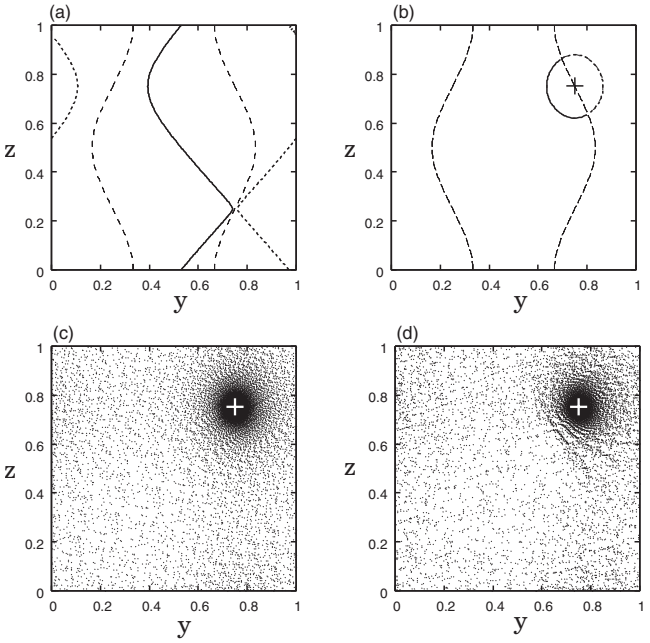

FIG. 4. Stable (solid line) and unstable (dotted line) fixed points located on invariant curves for (a) $V=0.666$, $\Omega=0.02$ prior to the first collision of fixed points, and for (b) $V=0.666$, $\Omega=0.165$ beyond the beginning of the collision. In (a) and (b), the dashed lines are critical curves $\Lambda(y,z)=0$, with contraction inside the two dashed lines and expansion outside. (c) 2-torus for $V=0.3$, $\Omega=\Omega_b(0.3)+10^{-6}$ just outside the boundary. (d) SNA for $V=0.666$, $\Omega=\Omega_b(0.666)+10^{-6}$. Plus (+) in each figure represents the position $(y,z)=(3/4,3/4)$ at which the last pair of stable and unstable fixed points annihilates.

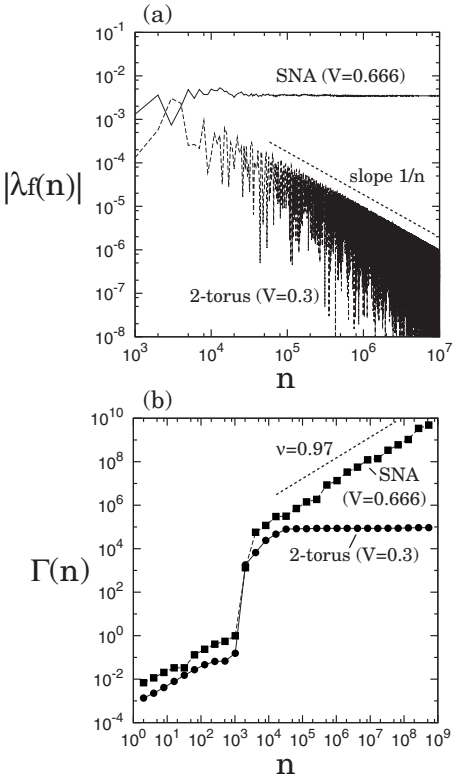

FIG. 5. (a) Convergence of the finite-time Lyapunov exponent $\lambda_f(n)$ for the 2-torus in Fig. 4(c) and for the SNA in Fig. 4(d). *Y* axis shows the absolute value $|\lambda_f(n)|$. (b) Phase sensitivity functions $\Gamma(n)$ for the same attractors in (a).

critical curves (dashed lines) as shown in Fig. 4(a). In contrast, for the parameters near the boundary $\frac{V}{2\pi}(1-\frac{\alpha}{k})\leq\Omega<\Omega_b(V)$, some of the stable and unstable fixed points annihilate each other on a critical curve, and the remaining fixed points form a ring-shaped invariant curve, as shown in Fig. 4(b). Upon further approaching the boundary, the ring-shaped invariant curve shrinks, accompanied by successive pair annihilations of stable and unstable fixed points, and finally at $\Omega=\Omega_b(V)$, the last pair of fixed points annihilates at $(y,z)=(3/4,3/4)$. As a result, several types of attractors such as 2-torus, SNA and chaotic attractor appear depending on the parameter values. Figure 4(c) shows a 2-torus with $\lambda_f=0$ and $\nu=0$ for $V=0.3$, $\Omega=\Omega_b(0.3)+10^{-6}$, and figure 4(d) shows an SNA with $\lambda_f\approx-0.003\,49$ and $\nu\approx0.97$ for $V=0.666$, $\Omega=\Omega_b(0.666)+10^{-6}$. To check that the 2-torus has $\lambda_f=0$ actually, we examine the convergence of finite-time Lyapunov exponent $\lambda_f(n):=\frac{1}{n}\Sigma_{j=0}^{n-1}\ln|f_x(x_j;\theta)|$. For the 2-torus, $\lambda_f(n)$ converges to zero as $|\lambda_f(n)|\sim1/n$ [see Fig. 5(a)]. Different behaviors of phase sensitivity function $\Gamma(n)$ for the attractors are shown in Fig. 5(b), where we can see a distinct power-law divergence $\Gamma(n)\sim n^{0.97}$ for the SNA and a saturation for the 2-torus.

There should be a question about whether SNAs arise in the immediate vicinity of the boundary $\Omega=\Omega_b(V)$ because there is also a dense set of *T*1 tongues. Figures 6(a) and 6(b) show the Lyapunov exponent λ_f and phase sensitivity exponent ν, respectively, as a function of $\Delta\Omega=\Omega-\Omega_b(V)$ for $V=0.3$ and $V=0.666$. For the case $V=0.666$, the phase sensi-

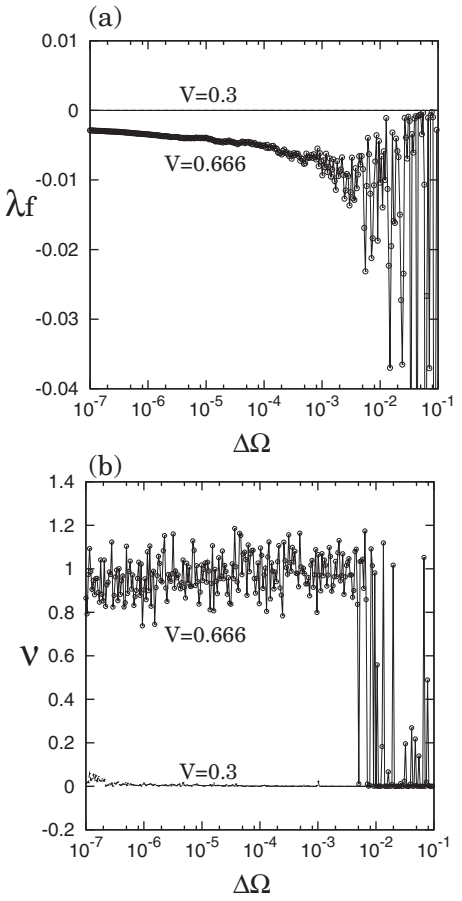

FIG. 6. (a) Lyapunov exponent λ_f vs $\Delta\Omega=\Omega-\Omega_b(V)$ and (b) phase sensitivity exponent ν vs $\Delta\Omega$ for $V=0.3$ (route a in Fig. 2) and $V=0.666$ (route b in Fig. 2).

tivity exponent ν maintains a value about 1.0 ± 0.3 for small $\Delta\Omega$. This result indicates that a lot of SNAs exist in the immediate vicinity of the boundary, with positive measure. Therefore, we conclude that SNAs can arise due to pair annihilation of fixed points.

After the transition, the dynamics show intermittency, where intermissions occur near the "ruin" of fixed points [see Figs. 4(c) and 4(d)]. The orbits of (y_n, z_n) in $\mathbb{T}^2$ are related to those of x_n in $\mathbb{R}$ by Eq. (10). In the latter, intermissions occur when x_n traverses narrow channels between map $f(x;\theta)$ and the bisector. Consider the case $\Omega>\Omega_b(V)$ and $V\leq V_c$ in which the map f is always above the bisector and monotonically increasing. Then x_n passes through all unit intervals defined by $I_m:=[m,m+1)$ with $m\geq\lfloor x_0\rfloor$ in the time course, where $\lfloor x_0\rfloor$ is the maximum integer less than x_0. We define the residence time $T_m(x_0,\theta)$ as the time interval during which the trajectory x_n stays in I_m,

$$T_m(x_0,\theta) := \min\{n|x_n \geq m+1\} - \min\{n|x_n \geq m\}. \quad (16)$$

The residence times $T_m(x_0,\theta)$ depend on the initial condition x_0 and parameter θ, but have an ergodic distribution function. As derived in the Appendix, the maximum residence time $T_{\max}:=\max_{m\geq\lfloor x_0\rfloor} T_m(x_0,\theta)$ is estimated to be $T_{\max}\simeq[V(1+k\alpha)\Delta\Omega/\pi]^{-1/2}$, and the mean residence time $\langle T\rangle := \lim_{M\to\infty}(1/M)\Sigma_{m=\lfloor x_0\rfloor}^{M} T_m(x_0,\theta)$ has a *logarithmic singularity* to the parameter $\Delta\Omega$,

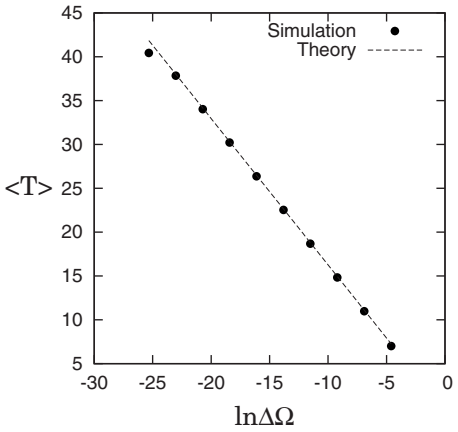

FIG. 7. Mean residence time (filled circles) in unit intervals. Dashed line shows the theoretical estimate in Eq. (17). A deviation from the theoretical line in $\ln\Delta\Omega<-25$ is due to poor statistics.

$$\langle T\rangle \simeq -c\ln\Delta\Omega - c\ln p, \quad (17)$$

where $c=\frac{1}{V}\sqrt{\frac{k}{\alpha}}$ and $p=\frac{\alpha\pi V}{k(1+k\alpha)}$. Similarly, rotation numbers W_y and $W_z(=kW_y)$ also have a logarithmic singularity to $\Delta\Omega$ since the rotation number of y is written as $W_y=1/\langle T\rangle$. Figure 7 shows a good correspondence between Eq. (17) and numerical simulations. Just on the boundary $\Omega=\Omega_b(V)$, rotation numbers W_y and W_z are both zero (because $\langle T\rangle=\infty$), but they show anomalous convergence obeying a nested logarithmic formula as reported in [35].

The existence of intermittency leaves a trace in the phase sensitivity function $\Gamma(n)$ in Fig. 5(b). At any time, x_n is either attracted to the nearest channel or repelled from it. In the attracting regimes, the derivative $f_x(x_n;\theta)$ is smaller than 1, and the phase sensitivity $\partial x_n/\partial\theta$ is reduced by Eq. (14). Contrarily, in the repelling regimes, the derivative $f_x(x_n;\theta)$ is greater than 1, and the phase sensitivity $\partial x_n/\partial\theta$ is expanded. In the ensemble of trajectories, there can be the one which is always attracted to a channel during half the period of the maximum residence time $[0,T_{\max}/2)$. This trajectory would give a small (almost minimal) phase sensitivity $|\partial x_n/\partial\theta|$ until $n\simeq T_{\max}/2$. However, since attracting regimes cannot last longer than $T_{\max}/2$, every trajectory with length $n>T_{\max}/2$ experiences repelling regimes in which the phase sensitivity $\partial x_n/\partial\theta$ is expanded. This is why the phase sensitivity function $\Gamma(n)$ increases suddenly near $n\approx T_{\max}/2(\approx 10^3)$ for both the 2-torus and SNA.

V. SUMMARY AND DISCUSSION

We have investigated Badard's non-skew-product map derived from a periodically driven dynamical system with spatially quasiperiodic potential. The strangeness of attractors has been characterized by the phase sensitivity exponent via its topologically conjugate map. We present a type of intermittency route to SNAs, where intermittent SNAs appear after pair annihilations of stable and unstable fixed points located on a ring-shaped invariant curve, and then the mean

residence time and rotation numbers have a logarithmic singularity. We have verified this type of intermittent transition to SNAs in other spatially quasiperiodic systems with continuous periodic forcing, for example, $\ddot{\phi}=-\eta\dot{\phi}+T-\sin\phi-a\sin(k\phi+\delta)+A\sin\omega t$. In this paper, we have limited our study to the phenomena observed in the invertible regime of map $\tilde{M}$. In noninvertible regime, we encounter more various bifurcations phenomena, for example, the torus fractalization to SNAs [15] and the period-doubling route to chaos [34].

Badard's map can be treated in a somewhat general framework. Consider a special class of non-skew-product maps on $\mathbb{T}^2$,

$$y_{n+1}=y_n+\Omega_y+F(y_n,z_n),$$

$$z_{n+1}=z_n+\Omega_z+kF(y_n,z_n), \tag{18}$$

where $F(y,z)$ is a periodic function in y and z, and the parameters Ω_y, Ω_z and k are arbitrary real numbers. In a manner explained in Sec. III, one can prove that there always exists a Lyapunov exponent of zero for this class of maps. By a homeomorphism $(x_n,\theta_n)=(y_n,z_n-ky_n)$, this class of maps is transformed into another class of skew-product maps on a cylinder $\mathbb{R}^1\times\mathbb{T}^1$,

$$x_{n+1}=x_n+\Omega_y+F(x_n,kx_n+\theta_n),$$

$$\theta_{n+1}=\theta_n+\omega,$$

where $\omega=\Omega_z-k\Omega_y$. Badard's non-skew-product map corresponds to the special case that k is irrational and $\omega=0$. If ω is irrational, we obtain quasiperiodically driven maps which typically exhibit SNAs. If ω is rational, we obtain periodically driven maps which may give rise to SNAs by choosing some irrational k. Therefore, we conjecture that the class of non-skew-product maps in Eq. (18) can exhibit SNAs for suitable functions F.

APPENDIX: DERIVATION OF THE MAXIMUM RESIDENCE TIME AND THE MEAN RESIDENCE TIME

In the situation that the parameter Ω be just greater than $\Omega_b(V)[:=\frac{V}{2\pi}(1+\frac{\alpha}{k})]$, and $V\le V_c[:=1/(1+\alpha)]$, map $f(x;\theta)$ in Eq. (8) has no fixed point and is monotonically increasing, but the orbit x_n takes many iterations to traverse narrow channels between the map function and the bisector. In these channels, both sinus values in the map approach -1 simultaneously. Thus, channel regions must be at least near $x\approx 3/4+m$ $(m\in\mathbb{Z})$. Taking a variable $\tilde{x}=x-(3/4+m)$ in each unit interval $I_m=[m,m+1)$, local behavior near a narrow channel is approximated by a differential equation

$$\frac{d\tilde{x}}{dn}\approx\Omega+\frac{V}{2\pi}\left[-\cos 2\pi\tilde{x}+\frac{\alpha}{k}\sin[k(\tilde{x}+3/4+m)+\theta]\right],$$

$$=\Omega-\frac{V}{2\pi}\left[\cos 2\pi\tilde{x}+\frac{\alpha}{k}\cos 2\pi(k\tilde{x}+\varepsilon_m)\right],$$

where n is considered as a continuous variable, and the parameter sequence ε_m is defined by

$$\varepsilon_m:=\begin{cases}[k(3/4+m)+\theta-3/4]\pmod 1\\ \text{if } [k(3/4+m)+\theta-3/4]\pmod 1\le 1/2\\ [k(3/4+m)+\theta-3/4]\pmod 1-1\\ \text{if } [k(3/4+m)+\theta-3/4]\pmod 1>1/2\end{cases}.$$

This sequence ε_m is considered as a uniform rotation on a circle $(-1/2,1/2]$ by an irrational k, and its terms ε_m can be infinitely small, that is, $\liminf_{m\to\infty}|\varepsilon_m|=0$. For small $\tilde{x}$ and ε_m, the above differential equation is approximated by the following quadratic form:

$$\frac{d\tilde{x}}{dn}\approx\Delta\Omega+\frac{V}{2\pi}\left[(1+k\alpha)\left(\tilde{x}+\frac{\alpha\varepsilon_m}{1+k\alpha}\right)^2+\frac{\alpha\varepsilon_m^2}{k(1+k\alpha)}\right],$$

where $\Delta\Omega:=\Omega-\Omega_b(V)$. In the case of large intermission, the residence time T_m defined in Eq. (16) is dominated by the time near a channel. Hence, T_m is obtained by integrating the quadratic differential equation with respect to $\tilde{x}$ across $\tilde{x}=-\alpha\varepsilon_m/(1+k\alpha)$,

$$T_m\simeq\frac{\pi}{\sqrt{\pi V(1+k\alpha)\Delta\Omega+\alpha(\pi V\varepsilon_m)^2/k}}.$$

For $\varepsilon_m=0$, we have the maximum residence time

$$T_m\simeq\sqrt{\frac{\pi}{V(1+k\alpha)\Delta\Omega}}.$$

Since the sequence ε_m has a uniform density $P(\varepsilon)=1$ in $(-1/2,1/2]$ (index m is omitted), the mean residence time is obtained by the ensemble averaging with respect to ε,

$$\langle T\rangle\simeq c[\ln|\varepsilon+\sqrt{\varepsilon^2+\Delta\Omega/p}|]_{\varepsilon=-1/2}^{\varepsilon=1/2}$$

$$\to -c\ln\Delta\Omega+c\ln p^{-1}(\Delta\Omega\to 0),$$

where $c=\frac{1}{V}\sqrt{\frac{k}{\alpha}}$ and $p=\frac{\alpha\pi V}{k(1+k\alpha)}$.

[1] C. Grebogi, E. Ott, S. Pelikan, and J. A. Yorke, Physica D **13**, 261 (1984).

[2] F. J. Romeiras and E. Ott, Phys. Rev. A **35**, 4404 (1987).

[3] A. Bondeson, E. Ott, and T. M. Antonsen, Phys. Rev. Lett. **55**, 2103 (1985).

[4] J. A. Ketoja and I. I. Satija, Physica D **109**, 70 (1997).

[5] A. Prasad, R. Ramaswamy, I. I. Satija, and N. Shah, Phys. Rev. Lett. **83**, 4530 (1999); S. S. Negi and R. Ramaswamy, Phys. Rev. E **64**, 045204(R) (2001); S. Datta, A. Sharma, and R. Ramaswamy, *ibid.* **68**, 036104 (2003).

[6] V. S. Anishchenko, T. E. Vadivasova, and O. Sosnovtseva, Phys. Rev. E **54**, 3231 (1996); A. Pikovsky and U. Feudel, *ibid.* **56**, 7320 (1997); V. S. Anishchenko, T. E. Vadivasova, and O. Sosnovtseva, *ibid.* **56**, 7322 (1997).

[7] S. S. Negi and R. Ramaswamy, Pramana, J. Phys. **56**, 47 (2001).
[8] X. Wang, M. Zhan, C.-H. Lai, and Y.-C. Lai, Phys. Rev. Lett. **92**, 074102 (2004); X. Wang, Y.-C. Lai, and C.-H. Lai, Phys. Rev. E **74**, 016203 (2006).
[9] R. Badard, Chaos, Solitons Fractals **28**, 1327 (2006).
[10] R. Badard, Chaos **18**, 023127 (2008).
[11] M. Ding, C. Grebogi, and E. Ott, Phys. Rev. A **39**, 2593 (1989).
[12] A. Pikovsky and U. Feudel, Chaos **5**, 253 (1995).
[13] U. Feudel, J. Kurths, and A. Pikovsky, Physica D **88**, 176 (1995).
[14] U. Feudel, C. Grebogi, and E. Ott, Phys. Rep. **290**, 11 (1997).
[15] K. Kaneko, Prog. Theor. Phys. **71**, 1112 (1984); T. Nishikawa and K. Kaneko, Phys. Rev. E **54**, 6114 (1996).
[16] T. Yalçınkaya and Y.-C. Lai, Phys. Rev. Lett. **77**, 5039 (1996).
[17] A. Prasad, V. Mehra, and R. Ramaswamy, Phys. Rev. Lett. **79**, 4127 (1997); Phys. Rev. E **57**, 1576 (1998).
[18] A. Witt, U. Feudel, and A. Pikovsky, Physica D **109**, 180 (1997).
[19] P. Glendinning, Phys. Lett. A **244**, 545 (1998).
[20] R. Sturman, Phys. Lett. A **259**, 355 (1999).
[21] A. Venkatesan, M. Lakshmanan, A. Prasad, and R. Ramaswamy, Phys. Rev. E **61**, 3641 (2000).
[22] S. P. Kuznetsov, Phys. Rev. E **65**, 066209 (2002).
[23] S.-Y. Kim, W. Lim, and E. Ott, Phys. Rev. E **67**, 056203 (2003); S.-Y. Kim and W. Lim, J. Phys. A **37**, 6477 (2004).
[24] W. Lim and S.-Y. Kim, Phys. Lett. A **335**, 383 (2005).
[25] A. Venkatesan, K. Murali, and M. Lakshmanan, Phys. Lett. A **259**, 246 (1999).
[26] W. L. Ditto, M. L. Spano, H. T. Savage, S. N. Rauseo, J. Heagy, and E. Ott, Phys. Rev. Lett. **65**, 533 (1990).
[27] T. Zhou, F. Moss, and A. Bulsara, Phys. Rev. A **45**, 5394 (1992).
[28] W. X. Ding, H. Deutsch, A. Dinklage, and C. Wilke, Phys. Rev. E **55**, 3769 (1997).
[29] U. Feudel, S. Kuznetsov, and A. Pikovsky, *Strange Nonchaotic Attractors* (World Scientific, Singapore, 2006).
[30] A. Prasad, S. S. Negi, and R. Ramaswamy, Int. J. Bifurcation Chaos Appl. Sci. Eng. **11**, 291 (2001); A. Prasad, A. Nandi, and R. Ramaswamy, *ibid.* **17**, 3397 (2007).
[31] Cantor attractors generated at accumulation points of period-doubling cascades are examples of SNAs. However, we can hardly observe such SNAs experimentally since the Lebesgue measure of accumulation points of period-doubling cascades is zero in parameter space.
[32] Skew-product maps are sometimes called autonomous maps in the literature since they are divided into a drive (θ) and a response (x) parts.
[33] If there exists a period-q cycle ($q \neq 1$), say (y_p, z_p), in map $\tilde{M}$, lift M satisfies $(y_p+m, z_p+l)=M^q(y_p, z_p)$ for some $m, l \in \mathbb{N}$. All variables of lift M must satisfy the restraint of Eq. (9), but the two points (y_p, z_p) and (y_p+m, z_p+l) cannot satisfy Eq. (9) simultaneously because this leads to a contradiction, $k=l/m$. Hence map $\tilde{M}$ has no cycle.
[34] T. Mitsui and Y. Aizawa (unpublished).
[35] T. Mitsui, Phys. Rev. E **78**, 026206 (2008).